IJAME
Int. J. of Applied Mechanics and Engineering, 2024, vol.29, No.1, pp.1-18
DOI: 10.59441/ijame/181643

CONJUGATE MIXED CONVECTION OF A MICROPOLAR FLUID OVER A VERTICAL HOLLOW CIRCULAR CYLINDER

Alliche Sid Ahmed, Bennia Ayoub and Bouaziz Amina Manal
Mechanical Engineering, University of Medea, ALGERIA

Bouaziz Mohamed Najib*
Mechanical Engineering, Biomaterials and Transport Phenomena, ALGERIA
E-mail: mn_bouaziz@email.com

This work conducts a numerical examination into the influence of a magnetic field and viscosity dissipation on the movement of a micropolar fluid over the surface of a vertical, hollow circular cylinder via conjugate mixed convection. In this investigation, we obtained a numerical solution for a non-linear differential equations-based modeling system by employing MATLAB and the bvp4c solver, which operates on a two-equation model. We show graphically how micropolar materials, conjugate heat transfer, viscous energy dissipation, buoyancy factors and magnetic field affect the temperature at the interface, local skin friction and heat transfer. By contrasting the acquired results with those found in the published research, which exhibit a high degree of concordance, the validity of the methodology is proven. The findings indicate that the escalation of the Eckert number correlates with an increase in both interfacial temperature and skin friction, accompanied by a reduction in local heat transfer. Furthermore, elevated magnetic and buoyancy values amplify both skin friction and thermal transfer, contributing to a decrease in dimensionless interfacial temperature distributions.

Key words: micropolar fluid, conjugate heat transfer parameter, viscous dissipation, magnetic field, buoyancy effect, vertical hollow circular cylinder.

1. Introduction

The topic of conjugate heat transfer involves a comprehensive study of heat transfer during a solid surface and fluid flow. Heat exchangers, nuclear reactors and cooling systems are merely a few of the numerous possible applications where this phenomenon finds use in engineering and science [1]. As of now, micropolar fluids in real-world scenarios have largely been in the research and development phase, and practical applications are still under exploration (nuclear reactor cooling, lubrification…). Conjugate heat transfer over vertical cylinders is complex and should considered due to the presence of interacting fluids and the level of convection, but understanding it can help optimize designs, increase energy efficiency, and guarantee safe, effective operations across a variety of industries. Jilani *et al.* [1] conducted a numerical investigation using a finite-difference scheme to study heat transfer via combined forced convection as well as conduction on a vertically oriented cylinder with internal heat generation. Rani and Reddy [2] conducted a numerical study of combined effects of heat transfer and heat generation amid unsteady natural convection boundary layer movement around a vertically elongated, cylindrical shape with a hollow center. The study involves deriving and solving a set of non-dimensional governing equations using computational fluid dynamics (CFD) techniques. The findings indicate that as the parameters related to conjugate conduction or heat generation rise, the time needed for the system to reach a stable condition similarly increases. This observation highlights the significant influence of heat transfer and heat generation under the condition of a constant inner surface temperature. In their study, Kaya [3] examined the impact of wall conduction and a perpendicular uniform

* To whom correspondence should be addressed

magnetic field on steady heat transfer in a vertical, thin hollow cylinder, taking into account both convection and magnetohydrodynamics.

Interest in investigating the behavior of complex fluids with microstructural effects has increased in the past several years in the field of fluid dynamics. Micropolar fluids are a fascinating type of fluid because, in addition to their usual translational motion, they also display micro-rotational motions. Micropolar fluids are complicated fluids that are made up of stiff or random-orientation (spherical) particles floating in a viscous medium. The model doesn't take into account the deformation of these fluid particles [4]. The study of complex fluids, including liquid crystals, polymer solutions, and biological fluids, can benefit from micropolar fluid models because they provide a more nuanced description of the fluids' behavior than traditional Newtonian fluids. It was Eringen who originally came up with the idea of micropolar fluids [5, 6]. Micropolar fluid has applications, in engineering systems such as electronic component cooling, thermal energy storage and heat exchangers. Recently Ariman *et al.* Conducted an in-depth review on the uses of fluids in engineering and technology [7, 8]. In another study by Gorla and Takhar [9] the impact of curvature on the fluid flow in a laminar free convective boundary layer was investigated. Specifically, they examined how micropolar fluids behave inside a cylinder taking into account the rotational properties of particles within the fluid. The findings suggest that compared to fluids micropolar fluids exhibit reduced drag and slower surface heat transfer. The study also explored conditions, like isothermal wall conditions and constant surface heat flow circumstances. The findings indicate that there is a positive correlation between transverse curvature and heat transfer rate. Additionally, micropolar fluids exhibit a decrease in both drag and heat transfer surface rates in comparison to Newtonian fluids.

Gorla [10] conducted a numerical study on a micropolar fluid's mixed convection flow around a vertically translating cylinder. His research demonstrated that increasing the buoyancy force and surface transverse curvature leads to an escalation in shear stress on the wall and the rate of surface heat transfer.

Chang [11] studied how a micropolar fluid flowed vertically up a narrow hollow circular cylinder while being subjected to forced convection. The study included taking into account the implications of wall conduction and buoyancy. The influence of wall conduction on the heat and flow fields is more prominent in systems with stronger buoyancy effects, or higher Prandtl numbers. In contrast, it is less responsive in systems with a larger micropolar material parameter. Furthermore, a comparison was conducted with Newtonian fluid. The current micropolar fluid exhibited a rise in the temperature at the interface, a reduction in the skin friction, and a decline in the rate of heat transfer.

In their study [12], Siddiqa *et al.* looked at how conjugate free convection behaved on a flat, limited-vertical surface Immersed in a micropolar fluid and exposed to strong thermal radiation. They found that the shear stress and couple stress coefficients were reduced by *49.29%* and *85.25%*, respectively, while the heat transfer rate increased by about *136%* as a result of an increase in the micro-inertia density parameter.

A fascinating area of research is looking into how magnetic fields and micropolar fluid flow over a vertical cylinder can be used in heat exchangers, chemical processing, and microfluidic devices to make them work better and more efficiently. In their study, Bhargava and Rana [13] investigate the numerical modeling of 2D stable boundary layer equations in the context of mixed convective flow of a micropolar fluid along a vertically moving, slender, hollow circular cylinder, with due consideration to the effects of suction and variable electric conductivity. For the purpose of resolving the governing differential equations, the finite element approach is utilized. Their findings reveal that increased fluid injection leads to higher temperatures, and wall shear stress exhibits direct proportionality to the magnetic field parameter.

Reddy *et al.* [14]. conducted a study in which they employed numerical analysis to investigate the behavior of a square heated cylinder placed within a filled square enclosure with laminar micropolar fluid subject to the MHD effect. The study explored various dimensionless parameters, including the Rayleigh and Hartmann numbers ($103 \leq Ra \leq 106,\ 0 \leq Ha \leq 50$). The results revealed that a rise in the magnetic field caused the boundary thermal layer to disappear, when the vortex viscosity parameter simultaneously enhanced both the heat transfer rate. Saidoune *et al.* [15] conducted a numerical analysis to investigate the impact of chemical reactions and heat generation on the transfer of mass and heat in a laminar mixed convective flow along a thin vertical hollow cylinder, incorporating magnetohydrodynamics (MHD). Their numerical analyses within the specified parameter ranges consistently revealed that employing strong conjugate heat transfer had an adverse impact on both the Sherwood and Nusselt numbers. Similar adverse trends were observed in the behavior of

the skin friction factor. Alwawi *et al.* [16] investigate numerically the impact of magnetism on micropolar nanofluid in a horizontal circular cylinder under a consistent wall temperature. Two different metal oxide nanoparticles and nanoparticles of nonmetals are submerged in two distinct base fluids: CMC-water and fuel oil. The findings indicate that increasing the value of the mixed convection parameter leads to an increment in skin friction, velocity, and Nusselt number.

However, there are a number of contexts where a thorough understanding of heat generation and dissipation necessitates research into viscous dissipation in micropolar fluids. Heat transfer in cooling systems, polymer processing, and lubrication systems are just a few examples of where these systems might be put to use. When processing polymers, viscous energy dissipation is pivotal as an internal energy source that produces heat. As a result, the solidification process is prolonged, taking more time than necessary [17].

Kaya and Aydin [18] looked at how Joule heating and viscous energy dissipation affect the interaction between mixed convection and conduction along a vertical, hollow, thin cylinder. Anantha Kumar *et al.* [19] presented a numerical investigation of the nonlinear flow with convection of a micropolar fluid that conducts electricity over a thin, stretched surface. Joule heating, Viscous energy dissipation, non-uniform heat sources and sinks, thermal conductivity that varies with temperature, and thermal radiation are all factors in the study. Heat transfer is analyzed using a variant of Fourier's law. Lund *et al.* [20] presented a numerical investigation of the MHD flow of a micropolar fluid across a contracting surface. Kataria *et al.* [21] conducted a comprehensive analysis of the heat transmission properties and micropolar fluid flow across a stretching surface. This research explores the interaction between convective boundary conditions, viscous energy dissipation and thermal radiation.

The movement of a micropolar hydromagnetic fluid across a permeable membrane, which was undergoing either stretching or contracting, was investigated by Waini *et al.* [22]. The researchers examined the impacts of interaction between heat radiation, convective boundary conditions, and viscous energy dissipation using a sheet containing Al_2O_3 and Copper nanoparticles.

Existing literature indicates only a little amount of study has been devoted to the topic of how magnetohydrodynamics and viscous energy dissipation affect micropolar fluids flow around a vertical, thin, hollow circular cylinder. This research looks into how a magnetic field and viscous dissipation affect the flow of a micropolar fluid in conjugate mixed convection around a vertical, hollow, slender circular cylinder. Numerical solutions are found using MATLAB and the bvp4c solver once the equations that govern are converted into local non-similarity equations.

2. Problem description

A two-dimensional analysis of combined convection flow of a micropolar fluid along a vertical cylindrical hollow structure cylinder with dimensions L and an outer radius r_0 ($L >> r_0$) is illustrated in Figure 1. For this issue, we orient the x-axis vertically and the r-axis perpendicular to the cylinder. T_∞ and U_∞ represent the temperature and velocity of the micropolar fluid at some point far out of the cylinder. A constant temperature of T_0 is applied to the inner surface of the cylinder, where T_0 is greater than T_∞ ($T_0 > T_\infty$). With the exclusion of density variation within the buoyancy factor, all fluid parameters are assumed to be constant. The buoyancy force created by a temperature gradient among the cylinder's surface and the surrounding micropolar fluid drives the flow upwards. A homogeneous magnetic field with strength B_0 is exerted perpendicular to the cylinder. The resulting magnetic field is disregarded because the assumed magnetic Reynolds number is extremely low.

The governing equations, considering the aforementioned assumptions and employing a combination of boundary layer approximations and Boussinesq, can be denoted below [23].

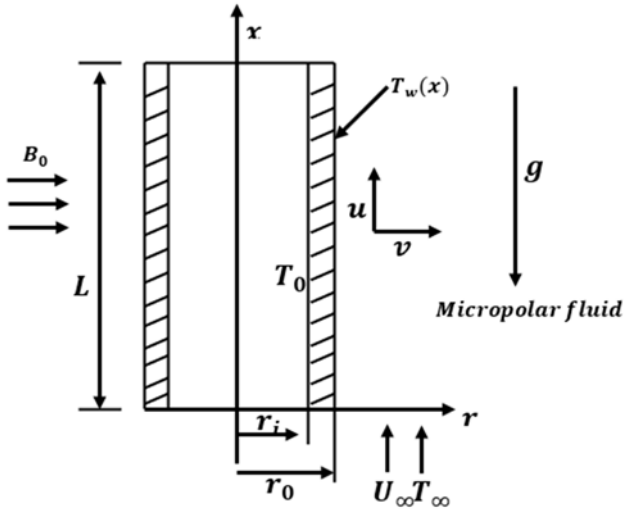

Fig.1. Displays the geometry being examined together with the coordinate and physical system.

Continuity:

$$\frac{\partial(ru)}{\partial x}+\frac{\partial(rv)}{\partial r}=0 \tag{2.1}$$

Momentum:

$$u\frac{\partial u}{\partial x}+v\frac{\partial u}{\partial r}=\left(\nu+\frac{k}{\rho}\right)\frac{1}{r}\frac{\partial}{\partial r}\left(r\frac{\partial u}{\partial r}\right)+\beta g\left(T-T_\infty\right)+\frac{k}{\rho}\left(\frac{N}{r}+\frac{\partial N}{\partial r}\right)-\frac{\sigma^* B_0^2}{\rho}\left(u-u_\infty\right). \tag{2.2}$$

Angular momentum:

$$u\frac{\partial N}{\partial x}+v\frac{\partial N}{\partial r}=\frac{\gamma}{j\rho}\left[\frac{1}{r}\frac{\partial}{\partial r}\left(r\frac{\partial N}{\partial r}\right)-\frac{N}{r^2}\right]-\frac{k}{j\rho}\left(\frac{\partial u}{\partial r}+2N\right). \tag{2.3}$$

Energy:

$$u\frac{\partial T}{\partial x}+v\frac{\partial T}{\partial r}=\left(\frac{\alpha}{r}\right)\frac{\partial}{\partial r}\left(r\frac{\partial T}{\partial r}\right)+\left(\frac{\nu}{Cp}\right)\left(\frac{\partial u}{\partial r}\right)^2+\frac{\sigma^* B_0^2}{\rho Cp}\left(u^2-u_\infty u\right). \tag{2.4}$$

In the equations above, the velocity components in the x and r dimensions are represented by the symbols u and v, respectively.

In addition, κ, j and γ discuss the fluid's microinertia density, spin-gradient viscosity, and vortex viscosity. T represent the fluid's temperature, B_0 stand for the magnetic flux density, N represent the direction of microrotation in the $(x-r)$ plane, and σ^* represent the fluid's electrical conductivity.

Equation (2.4) gives an energy equation that includes the effects of the Joule heating and viscous energy dissipation factor.

Conditions at those edges are:

$$r = r_0 : u = v = 0 \ , \quad N = -\frac{1}{2}\frac{\partial u}{\partial r} \ , \quad T = T_w(x), \tag{2.5.a}$$

$$r \to \infty : u = U_\infty \ , \quad N = 0, \quad T = T_\infty , \tag{2.5.b}$$

where the index w represents the wall and the index ∞ represents the edge of boundary layer.

The purpose of this research is to make educated guesses about how hot the cylinder's exterior will get. To accomplish this, an extra governing equation is necessary, assuming a consistent transfer of heat from the cylinder's wall to the surrounding micropolar fluid flow. In the heat conduction equation for the cylinder, the component representing axial conduction may be ignored due to the significant difference between the outer radius r_0 and the length L of the cylinder. As a result of this, Chang [11] has presented the equations that demonstrate the physical fluctuations of temperature within the cylinder.

$$\frac{1}{r}\frac{\partial}{\partial r}\left(r\frac{\partial T_S}{\partial r} \right) = 0, \quad 0 \le x \le L, \quad r_i < r \le r_0 . \tag{2.6}$$

The following boundary conditions that pertain to the cylinder wall:

$$\text{At} \quad r = r_i \, T_s = T_0 \tag{2.7.a}$$

$$\text{At the interface } r = r_0 : T_s = T(x, r_0), \quad -K_s \frac{\partial T_S}{\partial r} = -K_f \frac{\partial T(x, r_0)}{\partial r}. \tag{2.7.b}$$

Both the cylinder and the fluid have a certain thermal conductivity, denoted by K_s and K_f. The continuity of temperature and heat fluxes across the solid-fluid contact is established by the boundary conditions specified in Equation (2.7b). The interface temperature distribution, denoted as T_w, is subsequently calculated using Equations (2.6) and (2.7b).

$$T_w(x) = T(x, r_0) = r_0 \frac{K_f}{K_s} \ln\left(\frac{r_0}{r_i} \right) \frac{\partial T(x, r_0)}{\partial r} + T_0 . \tag{2.8}$$

To facilitate the resolution of the system of Eqs (2.1)-(2.4), the subsequent dimensionless variables are established:

$$\xi = \frac{x}{r_0}, \quad \eta = \frac{1}{2x} \mathrm{Re}_x^{1/2} \left(\frac{r^2 - r_0^2}{r_0} \right), \quad \varphi = r_0 \nu \, \mathrm{Re}_x^{1/2} F(\xi, \eta),$$

$$N = \frac{r_0 U_\infty^2}{\nu r} \mathrm{Re}_x^{-1/2} G(\xi, \eta), \quad \theta = \frac{T - T_\infty}{T_0 - T_\infty}, \tag{2.9}$$

where Re_x is the local Reynolds number;

$$Re_x = U_\infty \, x / \nu . \tag{2.10}$$

By including the stream function φ, the conservation equation is satisfied.

$$u = \frac{1}{r}\frac{\partial \varphi}{\partial r}, \quad v = -\frac{1}{r}\frac{\partial \varphi}{\partial x}. \tag{2.11}$$

By incorporating these supplementary variables, it is possible to represent the velocity components as follows:

$$u = U_\infty F', \qquad v = \frac{r_0}{r}\frac{\sqrt{\nu}\sqrt{U_\infty}}{\sqrt{x}}\left(\frac{1}{2}\eta F' - \frac{1}{2}F - \xi\frac{\partial F}{\partial \xi}\right) \tag{2.12}$$

The following set of ordinary differential equations is obtained by substituting equation (2.9) into equations (2.2) through (2.4).

$$\begin{aligned}&(1+\Delta)(1+\sigma\eta)F''' + (1+\Delta)\sigma F'' + \frac{1}{2}FF'' + \Delta G' + Ri\,\xi\,\theta - Mn\,\xi(F'-1) = \\ &= \xi\left(F'\frac{\partial F'}{\partial \xi} - F''\frac{\partial F}{\partial \xi}\right),\end{aligned} \tag{2.13}$$

$$\begin{aligned}&\lambda(1+\sigma\eta)G'' + \frac{1}{2}FG' + \frac{1}{2}F'G - \frac{\Delta B}{2}\sigma^2 G - \frac{1}{4}\left(\frac{\sigma}{1+\sigma\eta}\right)FG + \frac{1}{4}\left(\frac{\sigma}{1+\sigma\eta}\right)\eta F'G + \\ &-\frac{\Delta B}{4}\sigma^2(1+\sigma\eta)F'' = \xi\left[\frac{1}{2}\left(\frac{\sigma}{1+\sigma\eta}\right)G\frac{\partial F}{\partial \xi} + F'\frac{\partial G}{\partial \xi} - G'\frac{\partial F}{\partial \xi}\right],\end{aligned} \tag{2.14}$$

$$\begin{aligned}&\frac{1}{Pr}(1+\sigma\eta)\theta'' + \frac{1}{Pr}\sigma\theta' + \frac{1}{2}F\theta' + Ec(1+\sigma\eta)(F'')^2 + Mn\,Ec\zeta F'(F'-1) = \\ &= \xi\left(F'\frac{\partial \theta}{\partial \xi} - \theta'\frac{\partial F}{\partial \xi}\right),\end{aligned} \tag{2.15}$$

where the prime symbol denoting differentiation with respect to η,

$$\Delta = \kappa/\rho\nu, \quad B = r_0^2/j, \quad \lambda = \gamma/(j\rho\nu), \quad \sigma = 2\sqrt{\xi}/\sqrt{Re}, \quad Re = U_\infty r_0/\nu,$$

$$Ri = Gr/Re^2, \quad Gr = \frac{g\beta r_0^3(T_0 - T_\infty)}{\nu^2}, \quad Mn = \frac{\sigma^* B_0^2 r_0}{\rho U_\infty}, \quad \Pr = \frac{\nu}{\alpha}r, \quad Ec = \frac{{U_\infty}^2}{Cp(T_0 - T_\infty)}.$$

These are the new boundary conditions:

$$\text{At } \eta = 0: F'(\xi,0) = 0, \quad F(\xi,0) = -2\xi\left.\frac{\partial F}{\partial \xi}\right|_{\eta=0}, \quad G(\xi,0) = -\frac{1}{2}F'',$$

$$\theta(\xi,0) - 1 = p\,\xi^{-\frac{1}{2}}\theta'(\xi,0). \tag{2.16.a}$$

$$\text{At } \eta \to \infty : F'(\xi,\infty) = 1\,,\quad G(\xi,\infty) = 0\,,\quad \theta(\xi,\infty) = 0\,, \tag{2.16.b}$$

where $p = \dfrac{K_f}{K_s}\ln\left(\dfrac{r_0}{r_i}\right) Re^{1/2}$.

The dimensionless distribution of temperature at the interface, the skin friction coefficient, and Nusselt number are the fundamental quantities of physical significance, and they are stated as follows:

$$\theta_w = \theta(\xi,0) = \frac{T_w - T_\infty}{T_0 - T_\infty}, \tag{2.17}$$

$$C_f = 2\tau_w / \rho U_\infty^2, \qquad Nu_x = x\, q_w / K_f (T_0 - T_\infty)\,, \tag{2.18}$$

where the surface heat flux q_w and wall shear stress τ_w are expressed as:

$$\tau_w = \left[(\rho\nu + \kappa)\left(\frac{\partial u}{\partial r}\right) + \kappa N \right]_{r=r_0}, \quad q_w = -K_f \left(\frac{\partial T}{\partial r}\right)_{r=r_0} . \tag{2.19}$$

Equation (2.19) is obtained by substituting similarity transformations with Eq.(2.18).

$$C_f Re_x^{1/2} = 2\left(1 + \frac{\Delta}{2}\right) F''(\xi,0), \quad Nu_x\, Re_x^{-1/2} = -\theta'(\xi,0)\,. \tag{2.20}$$

2.1. Model for local similarities

For the first truncation or local similarity solution, $\xi \dfrac{\partial}{\partial \xi}$ terms in the governing Eqs (2.13), (2.14), and (2.15) are ignored on the assumption that they are minor. This is truer than ever when $\xi \ll 1$. Disregarding these terms yields the collection of equations of ordinary differential type along with their corresponding boundary conditions (2.16.a) and (2.16.b).

$$(1+\Delta)(1+\sigma\eta) F''' + (1+\Delta)\sigma F'' + \frac{1}{2} FF'' + \Delta G' + Ri\,\xi\,\theta - Mn\,\xi(F' - 1) = 0\,, \tag{2.21}$$

$$\begin{aligned} &\lambda(1+\sigma\eta) G'' + \frac{1}{2} FG' + \frac{1}{2} F'G - \frac{\Delta B}{2}\sigma^2 G - \frac{1}{4}\left(\frac{\sigma}{1+\sigma\eta}\right) FG + \\ &+ \frac{1}{4}\left(\frac{\sigma}{1+\sigma\eta}\right)\eta F'G - \frac{\Delta B}{4}\sigma^2 (1+\sigma\eta) F'' = 0, \end{aligned} \tag{2.22}$$

$$\frac{1}{Pr}(1+\sigma\eta)\theta'' + \frac{1}{Pr}\sigma\theta' + \frac{1}{2} F\theta' + Ec(1+\sigma\eta)(F'')^2 + Mn\, Ec\zeta F'(F' - 1) = 0\,, \tag{2.23}$$

with the boundary conditions:

$$\text{At } \eta = 0 : F'(\xi,0) = 0 , \quad F(\xi,0) = 0 , \quad G(\xi,0) - \frac{1}{2} F'' ,$$

$$\theta(\xi,0) - 1 = p\,\xi^{-\frac{1}{2}}\,\theta'(\xi,0) . \tag{2.24.a}$$

$$\text{At } \eta \to \infty : F'(\xi,\infty) = 1 , \quad G(\xi,\infty) = 0 , \quad \theta(\xi,\infty) = 0 . \tag{2.24.b}$$

2.2. Models with local non-similarity

By defining the variables $H = \partial F / \partial \xi$, $K = \partial G / \partial \xi$ and $L = \partial \theta / \partial \xi$ and differentiating the Eqs (2.13)-(2.15) with respect to ξ and ignoring the terms $\partial H / \partial \xi$, $\partial K / \partial \xi$ and $\partial L / \partial \xi$, the governing equations for the two-equation models with local non-similarities can be written as follows:

$$\begin{aligned}
&(1+\Delta)(1+\sigma\eta) H''' + (1+\Delta)\left(\frac{\eta}{\sqrt{\xi}\sqrt{Re}} \mathrm{F}''' \right) + (1+\Delta)\frac{2}{\sqrt{Re}}\left(H''\sqrt{\xi} + \frac{1}{2\sqrt{\xi}} F'' \right) + \\
&+ \frac{1}{2}(H F'' + F H'') + \Delta K' + Ri(\theta + \xi L) - Mn(F' + \xi H') + Mn = \\
&= (F'H' - F''H) + \xi\left[\left(H'H' + F' \frac{\partial H'}{\partial \xi} \right) - \left(H''H + F'' \frac{\partial H}{\partial \xi} \right) \right],
\end{aligned} \tag{2.25}$$

$$\begin{aligned}
&\lambda(1+\sigma\eta) K'' + \lambda\left(\frac{\eta}{\sqrt{\xi}\sqrt{Re}} \mathrm{G}'' \right) + \frac{1}{2}(H G' + F K') + \frac{1}{2}(H'G + F'K) - \Delta B \frac{2}{Re}(G + \xi K) - \\
&+ \frac{1}{4}\left[\left(\frac{1}{\left(\sqrt{\mathrm{Re}}\sqrt{\xi}\right)(1+\sigma\eta)^2} \right) F G + H\left(\frac{\sigma}{1+\sigma\eta} \right) G + K\left(\frac{\sigma}{1+\sigma\eta} \right) F \right] + \\
&+ \frac{1}{4}\eta\left[\left(\frac{1}{\left(\sqrt{\mathrm{Re}}\sqrt{\xi}\right)(1+\sigma\eta)^2} \right) F'G + H'\left(\frac{\sigma}{1+\sigma\eta} \right) G + K\left(\frac{\sigma}{1+\sigma\eta} \right) F' \right] + \\
&- \frac{\Delta B}{Re}\left[\left(1 + 3\eta\frac{\sqrt{\xi}}{\sqrt{\mathrm{Re}}} \right) F'' + (1+\sigma\eta)\xi H'' \right] = \left[\frac{1}{2}\left(\frac{\sigma}{1+\sigma\eta} \right) G H + F'K - G'H \right] + \\
&+ \xi\left[\frac{1}{2}\left(\left(\frac{1}{\left(\sqrt{\mathrm{Re}}\sqrt{\xi}\right)(1+\sigma\eta)^2} \right) G H + K\left(\frac{\sigma}{1+\sigma\eta} \right) H \right) + H'K - K'H \right],
\end{aligned} \tag{2.26}$$

$$\begin{aligned}
&(1+\sigma\eta) L'' + \frac{\eta}{\sqrt{\xi}\sqrt{\mathrm{Re}}} \theta'' + \frac{2}{\sqrt{\mathrm{Re}}}\left(\frac{1}{2\sqrt{\xi}}\,\theta' + \sqrt{\xi} L' \right) + \frac{Pr}{2}(H\theta' + F L') + \\
&+ \mathrm{Pr} Ec\left[\left(\frac{\eta}{\sqrt{\xi}\sqrt{Re}} (F'')^2 \right) + 2\left((1+\sigma\eta) F'' H'' \right) \right] + \\
&+ \mathrm{Pr}\, Mn\, Ec\left[\left((F')^2 + 2\left(\xi F' H' \right) \right) - (F' + \xi H') \right] = \mathrm{Pr}\left[(F'L - \theta' H) + \xi(H'L - L'H) \right].
\end{aligned} \tag{2.27}$$

The boundary conditions now become

$$\text{At } \eta = 0 : H'(\xi,0) = 0 ,\ \ H(\xi,0) = 0 ,\ \ K(\xi,0) = -\frac{1}{2}H'',\ \ L(\xi,0) - p\left[\frac{L'\sqrt{\xi} - \frac{1}{2\sqrt{\xi}}\theta'}{\xi}\right] = 0. \tag{2.28}$$

$$\text{At } \eta \to \infty : H'(\xi,\infty) = 0,\ \ K(\xi,\infty) = 0,\ \ L(\xi,\infty) = 0. \tag{2.29}$$

3. Validation and numerical solution

Using MATLAB and the bvp4c solver, we numerically solve equations that govern (2.25)-(2.27) and the boundary conditions (2.28)-(2.29). Shampine *et al.* [24] provide a thorough description of the procedure for solving the problem. The coefficient of skin-friction $F''(\xi,0)$ and the Nusselt number $-\theta'(\xi,0)$ are compared to the prior work of Chen and Mucoglu [25] to test the numerical technique accuracy. The values in Tab.1 are sufficiently similar to prove that the derived equations and the code are both correct.
Table 1. illustrates a comparison between heat transfer and skin friction values found in previously published literature [25] for the following conditions: $\Pr = 0.7$, $Ri = 0$, $Mn = 0$, $Ec = 0$, $p = 0$ and $\Delta = B = \lambda = 0$.

Table 1. Comparison between heat transfer and skin friction values.

$\frac{4}{r_0}\left(\frac{vx}{U_\infty}\right)^{1/2}$	Chen and Mucoglu [25]		Present results	
	$F''(\xi,0)$	$-\theta'(\xi,0)$	$F''(\xi,0)$	$-\theta'(\xi,0)$
0.0	*1.3282*	*0.5854*	*1.3285*	*0.5855*
1.0	*1.9172*	*0.8669*	*1.9172*	*0.8669*
2.0	*2.3981*	*1.0968*	*2.3981*	*1.0968*
3.0	*2.8270*	*1.3021*	*2.8271*	*1.3025*
4.0	*3.2235*	*1.4921*	*3.2241*	*1.4935*

4. Discussion and results

This study visually analyzes the results of the combined convection flow conjugate of a micropolar fluid with conjugate effects over a vertical thin hollow cylinder. The analysis takes into account the impact of a viscous energy dissipation and magnetic field. (Figs 2-6). Parameters used included: $\lambda = 5.0$, $B = 1\times10^5$, $Re = 250$, $\Delta = 0.0 - 12.0$, $Pr = 10.0$, $Ri = 0.0 - 20.0$, $Mn = 0.0 - 2.0$, $P = 0.0 - 0.3$ and $Ec = 0.0 - 0.03$ (Positive values of *Ec* indicate a scenario of wall heating, where heat is conveyed from the walls into the fluid, particularly in cases where T_0 is greater than T_∞) [18].

In Fig.2.a, we see how the interfacial temperature varies with ξ as a function of the micropolar material parameter Δ. The graph distinctly illustrates that the non-dimensional temperature at the interface increases with the increment of ξ. Furthermore, due to their distinct microstructural features including micro-rotations and micro-inertias, micropolar fluids display greater interfacial temperatures compared to Newtonian fluids. These characteristics cause more fluid motion and mixing close to the contact, which boosts convective heat transfer and leads to higher temperatures at the interface. In addition, as the micropolar material parameter increases, the dimensionless interfacial temperature rises.

As shown in Fig2.b, the skin friction is affected by the micropolar material parameter for both $p = 0.0$ (solid lines) and $p = 0.2$ (dashed lines). It is clear that the microstructural features of micropolar fluids may cause them to have lower skin friction factors compared to Newtonian fluids. These characteristics encourage more constant fluid motion, better mixing, and flatter velocity profiles close to the surface. Reduced flow resistance and lower skin friction factors are the outcomes of these influences. Also, a lower skin friction factor is associated with a higher value of Δ. In addition, raising the parameter of conjugate heat transfer boosts heat transmission between the fluid and the solid surface. The end effect is altered behavior of the flow close to the surface and lower skin friction.

Figure 2.c shows how the worth of the micropolar material parameter affects the heat transmission at a specific location. When the micropolar parameter is raised, local heat transport is impaired. It is also demonstrated that micropolar fluids, in comparison to Newtonian fluids, have a decreased local heat transfer. This is because micro-rotations and micro-inertias in micropolar fluids create distinctive flow patterns and mixing behavior. These characteristics modify heat transfer rates by altering velocity and temperature distributions close to the cylinder's surface. Otherwise, a greater thermal gradient within the solid and different flow patterns in the fluid would arise from an elevation in the parameter for conjugate heat transfer. These modifications lessen the heat transfer across the system as a whole, including at the fluid-solid interface.

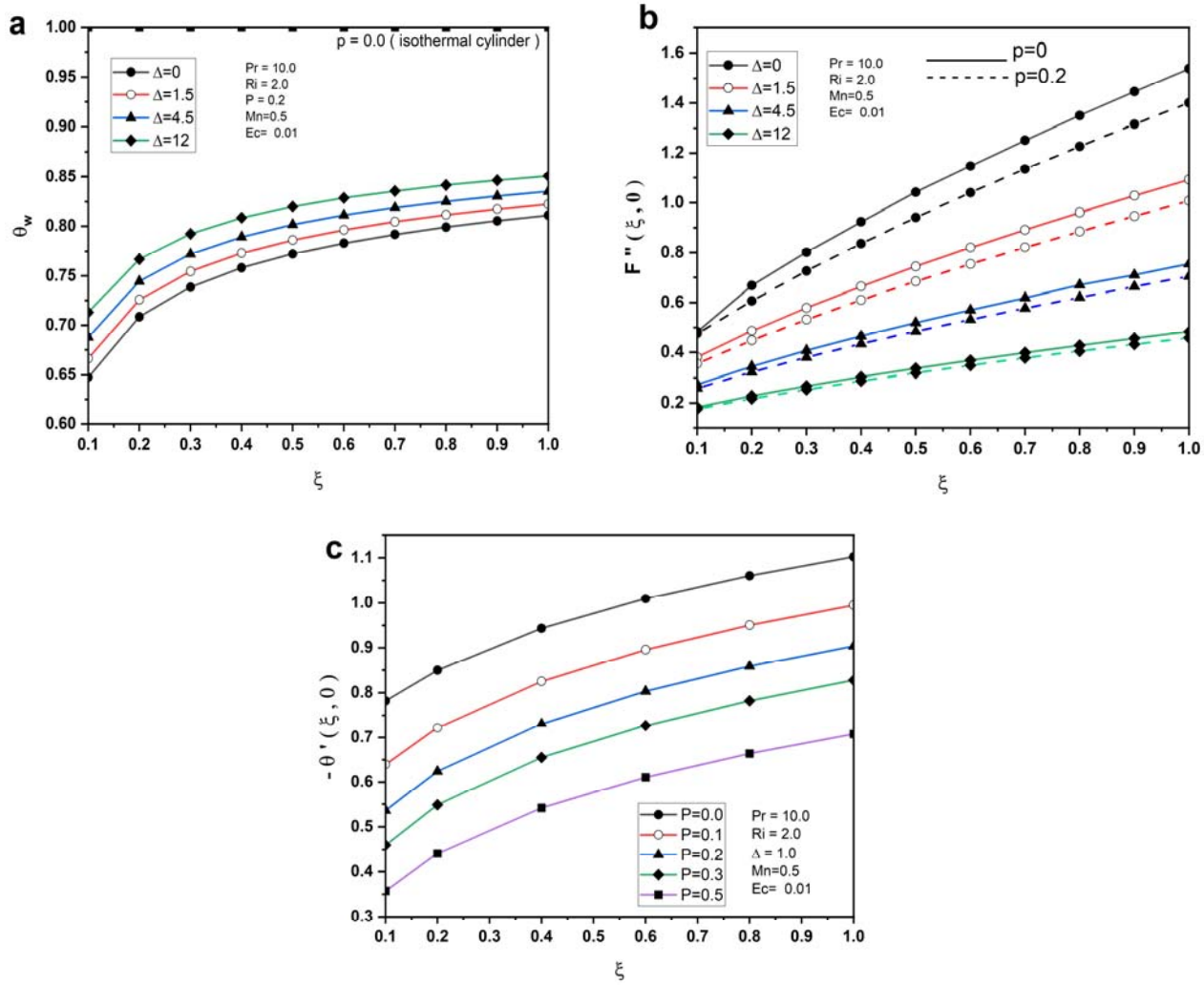

Fig.2. Impact of Δ on interface temperature (a), skin friction (b) and thermal transfer (c).

Figure 3.a shows variation in interfacial temperature based on the coupled heat transfer parameter. The fluid's surface temperature is shown to increase monotonically with ξ, indicating a stronger thermal interaction between the fluid and the solid surfaces as the conjugate heat transfer value rises. Enhanced contact leads to improved heat transfer from the fluid to the solid, resulting in cooling at the fluid-solid interface. This improved thermal contact leads to a reduction in interface temperature, demonstrating enhanced heat transfer as the fluid becomes more effective at transferring heat to the solid surface.

Local skin friction is shown to be affected by the conjugate heat transfer parameter in Fig.3.b. An escalation in the coupled heat transfer parameter leads to enhanced thermal contact between the micropolar fluid and the solid wall surface. The skin friction factor diminishes as a result of the changes in fluid flow patterns and boundary layer properties brought about by the enhanced heat contact near the surface.

Figure 3.c shows how the value of the local transfers of heat is influenced by the coupled heat transfer parameter ***p***. It can be seen that there is an augmentation of the rate of local transfer with ξ. It is also observed that the heat transfer drops off as the value of ***p*** rises. Conjugate heat transfer improves heat transmission to a solid surface, which can reduce the rate at which heat is lost from the fluid to its surroundings. This is due to the fact that a great deal of the heat is absorbed by the solid and then released as radiation at the solid's surface.

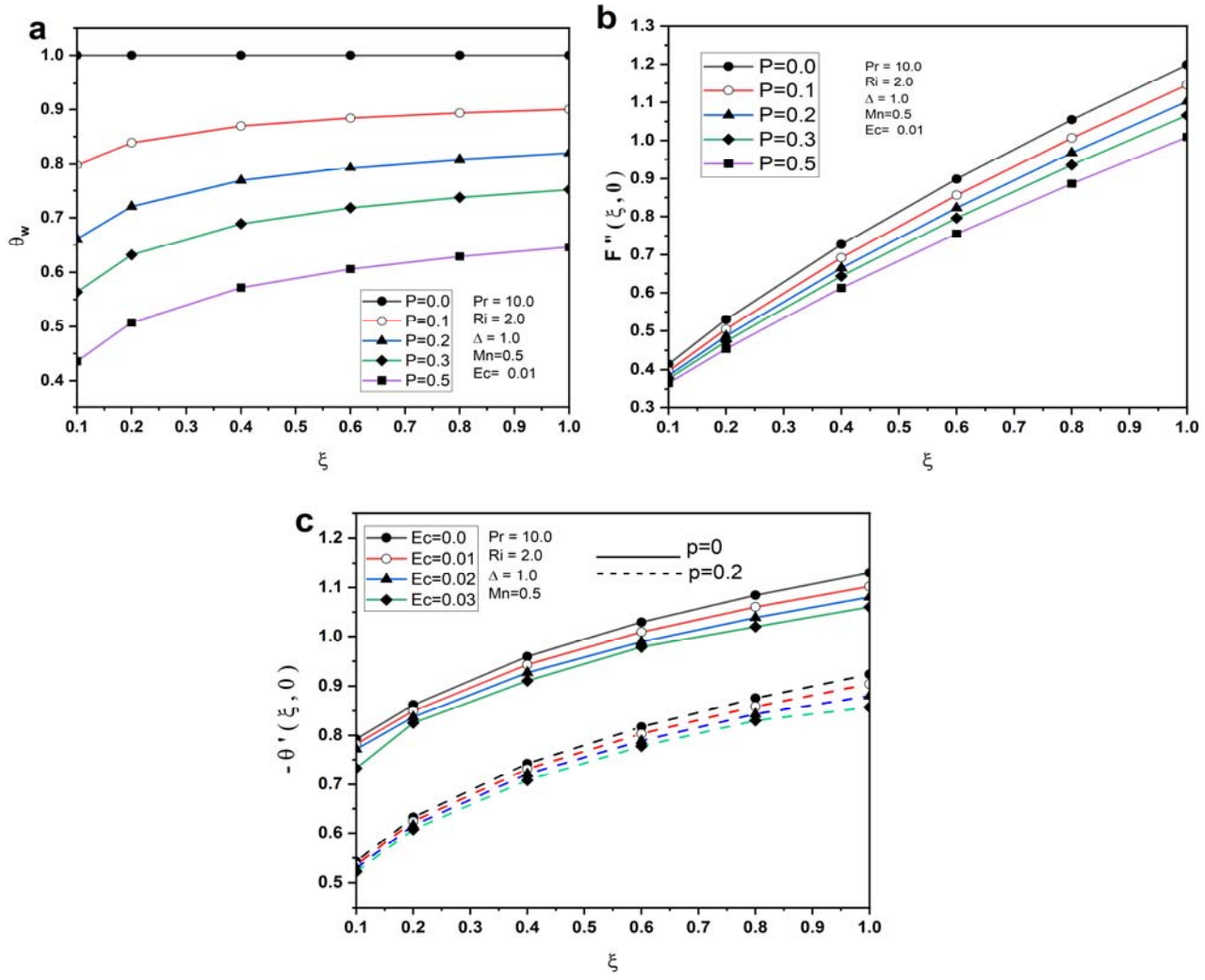

Fig.3. Effect of ***p*** on three parameters: interface temperature (a), skin friction (b) and thermal transfer (c).

Figure 4.a depicts how the interfacial temperature parameter fluctuates based on the Eckert number. An elevation in the Eckert number (where kinetic energy surpasses thermal energy) enhances fluid motion and mixing in proximity to the surface. This heightened fluid motion results in improved convective heat transfer, consequently leading to an elevation in the temperature at the interface.

The influence of the Eckert number ***Ec*** on the local skin friction is seen in Fig.4.b. A higher ***Ec*** signifies a prevalence of kinetic energy in the fluid flow over thermal energy. Consequently, this can lead to elevated shear stresses at the solid surface and increased flow velocities near the vertical cylinder's surface. As a result, skin friction escalates, resulting in increased resistance to flow along the surface. On the other hand, a non-isothermal cylinder exhibits a temperature gradient across its surface, altering fluid flow patterns and boundary layer formation. In comparison to a cylinder at constant temperature $(p=0)$, the presence of a temperature gradient modifies flow characteristics and leads to a decrease in skin friction.

As seen in Fig.4.c, the Eckert number significantly affects the local heat transmission. The thermal boundary layer is disturbed and the surface temperature gradients are reduced as the Eckert number rises. The local heat transfer rate drops because thermal convection slows from the fluid to the solid surface. The surface of a non-isothermal cylinder, on the other hand, experiences a temperature gradient. This temperature difference impacts convective heat transfer by changing the flow patterns. Local heat transfer rates are lower than they would be in an isothermal cylinder because of the existence of a temperature difference, which disturbs fluid flow and reduces thermal convection.

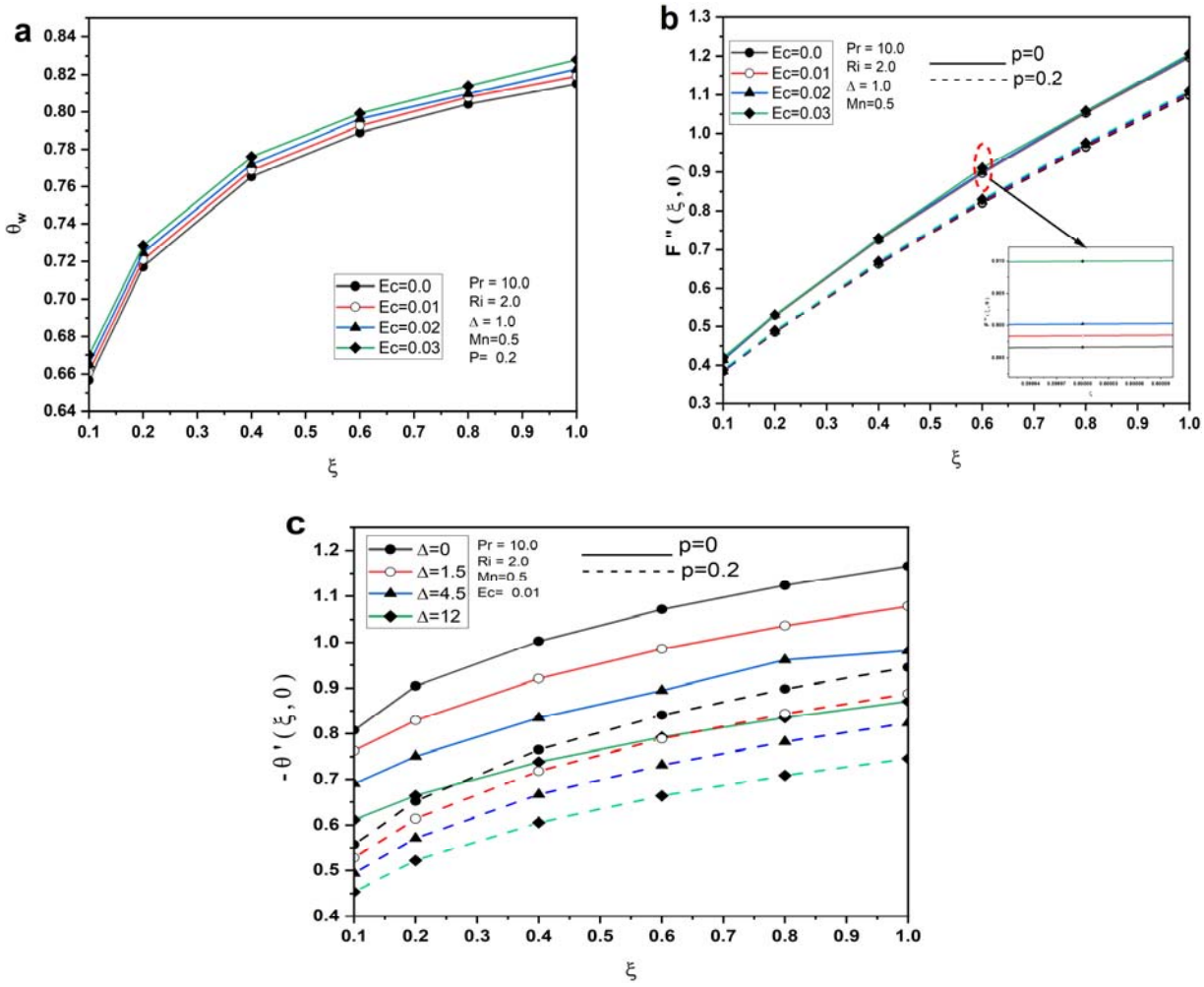

Fig.4. The influence of ***Ec*** on three variables: interface temperature (a), skin friction (b) and thermal transfer (c).

Figure 5.a shows how the parameter representing the magnetic field affects the change in the interfacial temperature. The fluid at the surface of the vertical cylinder experiences a force due to the magnetic field, causing the flow pattern to alter. Suppressing vortices, modifying boundary layer development, and increasing fluid mixing are all examples of the kinds of changes that can be made to boost thermal convection. As a result of this increased convective heat transfer, heat is more easily transferred from the fluid to the solid surface, resulting in a lower temperature at the interface.

Figure 5.b illustrates the impact of the magnetic field parameter on skin friction. As shown, the skin friction rises alongside the magnetic parameter. A higher magnetic field intensifies the fluid-solid interaction, which in turn exerts more drag on the surface-flowing fluid. As a result, local skin friction increases and flow resistance rises. Local skin friction for an isothermal cylinder is typically greater than that for a non-isothermal cylinder due to the additional fluid resistance caused by the Lorentz force, which acts independently of the magnetic field and the temperature distribution.

Figure 5.c shows how the magnetic field parameter affects heat transmission at the local level. In general, the local heat transfer of a micropolar fluid improves as the magnetic parameter is increased. The presence of a magnetic field generates Lorentz forces, resulting in an impact on thermal conduction and fluid dynamics. These forces boost the effectiveness of thermal convection by increasing the rate at which fluids are moving. Also, convective heat transfer rates are higher in an isothermal cylinder than in a non-isothermal cylinder because of the magnetic field and the lack of a temperature difference. When compared to an isothermal cylinder, local heat transfer rates may be reduced because of the existence of a magnetic field, which interacts with the temperature distribution.

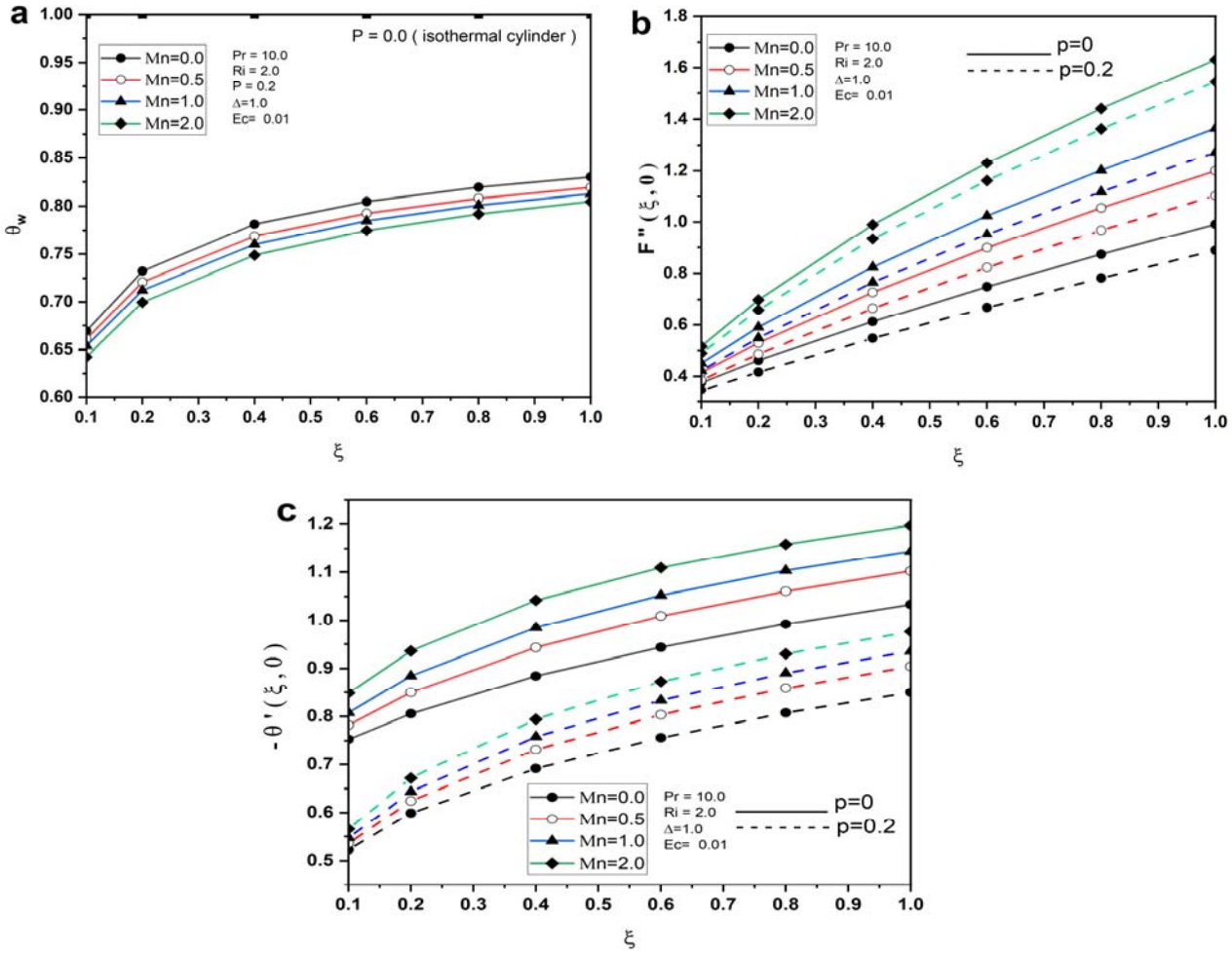

Fig.5. The influence of ***Mn*** on three variables: interface temperature (a), skin friction (b) and thermal transfer (c).

Figures 6.a show how the buoyancy force affects the changes in temperature at the interface. If the Richardson number is raised, natural convection speeds up. Thermal energy moves more efficiently from the fluid to the solid surface when buoyant forces, driven by temperature differences, become more pronounced, causing fluid motion. The temperature at the interface drops because the fluid is being convected and mixed, which removes heat from the interface.

The effect of the buoyancy force on local skin friction is seen in Fig.6.b. As the buoyancy effect gets stronger, buoyancy-driven convection takes over and changes how the flow and boundary layer behave close to the surface of the cylinder. The increased skin friction is a direct outcome of the greater flow velocities caused by the heightened fluid motion. The increased shear stresses along the surface caused by the higher fluid motion increase the local skin friction factor and the resistance to flow. When the buoyancy effect and temperature distribution are both taken into account, the local skin friction for an isothermal cylinder tends to be bigger. This is because buoyancy-driven convection causes the fluid to move more.

Figure 6.c shows how the buoyancy force affects the local heat transfer. The buoyancy effect is amplified due to temperature fluctuations, which have a major impact on local heat transfer. Fluid motion is induced by buoyancy-driven convection, which changes flow patterns close to the surface. Stronger buoyancy effects cause greater fluid motion, which in turn improves mixing and heat transfer between the fluid and the solid surface. As a result of the enhanced fluid velocity, local heat transfer rates are improved. In addition to increasing heat transmission via convective heat transport, the buoyancy effect also affects the growth of the boundary layer, modifying its thickness and properties. The buoyant forces, on the other hand, boost fluid motion in an isothermal cylinder, leading to enhanced mixing and enhanced heat transfer from the fluid to the solid surface. Isothermal cylinders have greater local heat transfer than non-isothermal cylinders because of this.

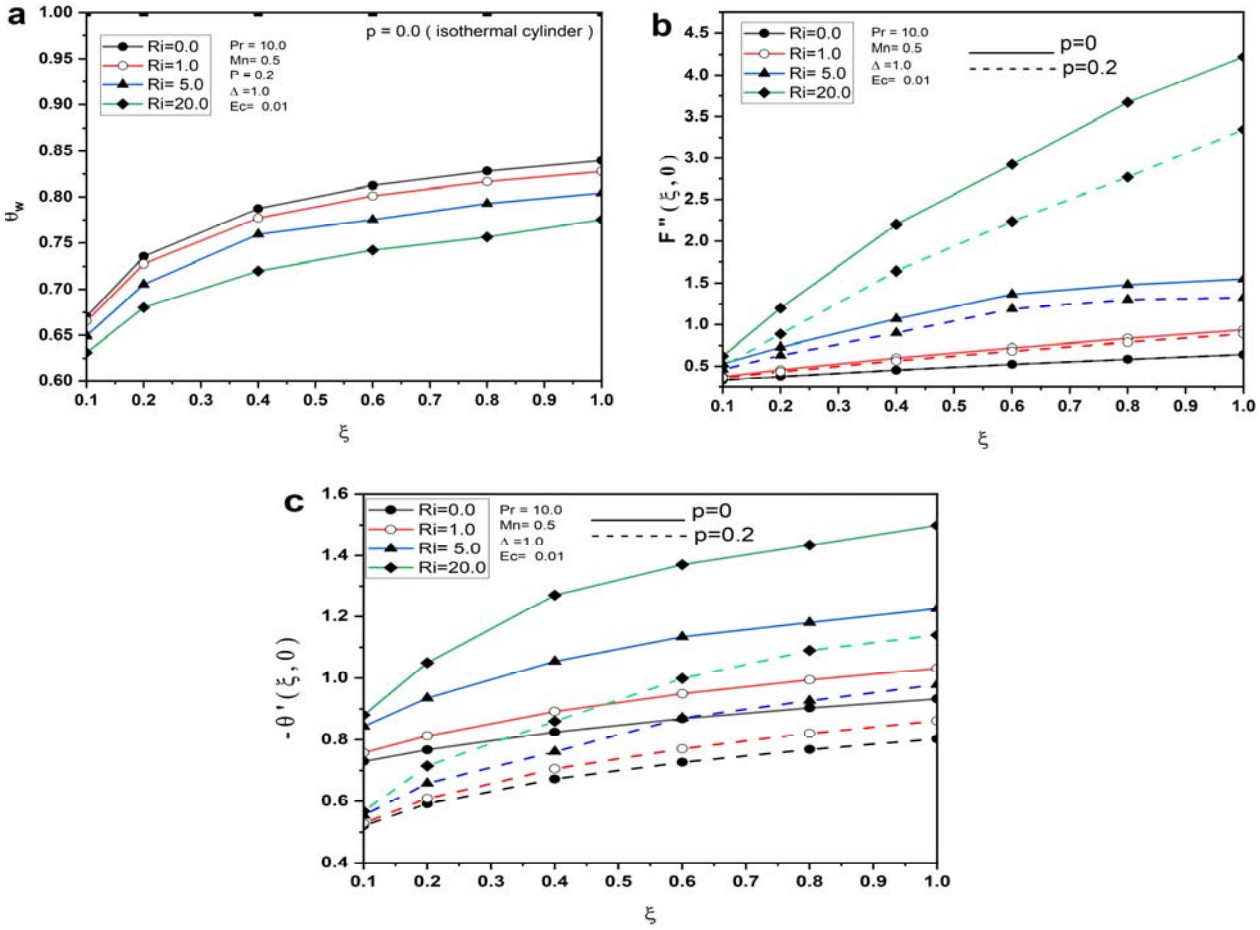

Fig.6. The influence of ***Ri*** on three variables: interface temperature (a), skin friction (b) and thermal transfer (c).

5. Conclusion

This investigation delves into the intricate dynamics governing the mixed convection flow of a micropolar fluid around a vertical, hollow, circular cylinder, with a specific focus on the impact of a magnetic field and viscous dissipation. Employing a sophisticated two-equation modeling approach, the study rigorously formulates and solves the nonlinear governing equations that describe the complex fluid behavior. A meticulous consideration of the pertinent boundary conditions is undertaken to ensure a comprehensive analysis. The computational aspects of this research involve utilizing MATLAB software to meticulously calculate and derive the mathematical solution results, shedding light on the nuanced interplay of magnetic and viscous forces for micropolar fluid flow within this unique configuration.

An examination of the distribution of interfacial temperature between the solid wall and liquid phases is conducted, encompassing a comprehensive analysis of skin friction and thermal transfer phenomena. This investigation delves into the intricate dynamics influenced by diverse characteristics such as micropolar physical properties, conjugate heat transfer processes, the dissipation of viscosity, the influence of a magnetic field, and the impact of buoyancy. The resultant findings of this study can be succinctly encapsulated in the following summary:

1. As the micropolar material parameter experiences an augmentation, a notable reduction is discerned in both skin friction and thermal transfer. It is crucial to underscore that this escalation in the micropolar material parameter simultaneously gives rise to an elevation in the dimensionless temperature. Additionally, in the comparative analysis between micropolar fluids and Newtonian fluids, it is evident that micropolar fluids manifest higher interfacial temperatures while concurrently displaying lower magnitudes of skin friction and heat transfer. An intriguing observation emerges, indicating that the augmentation of the heat transfer parameters yields a corresponding reduction in both skin friction and heat transmission. This suggests a complex interplay of factors influencing the thermal and frictional characteristics of micropolar fluid flow.
2. When we increase the parameter of conjugate heat transfer, we observe a decrease in the temperature, skin friction, and thermal transfer rate.
3. An escalation in the Eckert number results in heightened interfacial temperature and increased skin friction. As the Eckert number rises, there is a corresponding reduction in local heat transfer. Furthermore, a non-isothermal cylinder exhibits lower skin friction and heat transfer in comparison to an isothermal cylinder.
4. Interfacial temperature and skin friction both rise when the Eckert number rises. When the Eckert number increases, however, local heat transmission diminishes. The skin friction and thermal transfer of a non-isothermal cylinder are also smaller than those of an isothermal cylinder.
5. Elevated magnitudes of magnetic and buoyancy values result in heightened skin friction and thermal transfer parameters, concurrently reducing dimensionless interfacial temperature distributions. Additionally, in comparing an isothermal cylinder to a non-isothermal counterpart, the former exhibits elevated values of skin friction and thermal transfer.

It should be boted that some fluids having a significant micropolarity accompanied by a specific rheology can be the subject of a similar examination.

Acknowledgements

This work was supported by the Biomaterials and transport phenomena laboratory agreement This work was supported in entire part by the Biomaterials and transport phenomena laboratory agreement N° 303 03-12-2003, at University Yahia Fares of Medea. The authors acknowledge and gratefully thank the financial support provided by DG-RSDT of Algeria and appreciate the constructive comments of the reviewers which led to definite great improvement in the paper.

Nomenclature

B – dimensionless parameter of microinertia density
B_0 – magnetic flux density
C_f – skin-friction coefficient
Cp – specific heat at constant pressure
Ec – Eckert number
F – reduced stream function
g – gravitational acceleration
G – dimensionless micro-rotation
Gr – Grashof number
j – microinertia density
k – thermal conductivity
L – length of the cylinder
Mn – magnetic parameter
N – angular velocity of micropolar fluid
Nu_x – local Nusselt number
P – conjugate heat transfer parameter
Pr – Prandtl number
q_w – surface heat flux
r_i, r_0 – inner and outer radius of the cylinder
Re – Reynolds number
Re_x – local Reynolds number
Ri – Richardson number
T – temperature
u, v – velocities in x and r directions
x, r – coordinates in axial and radial directions

Greek symbols

α – thermal diffusivity
β – coefficient of thermal expansion
γ – spin-gradient viscosity
Δ – dimensionless parameter of vortex viscosity
η – pseudo-similarity variable
θ – dimensionless temperature
κ – vortex viscosity
λ – dimensionless parameter of spin-gradient viscosity
ν – kinematic viscosity
ξ – dimensionless stream wise coordinate
ρ – fluid density

σ – transverse curvature parameter

σ^* – electrical conductivity of the fluid

τ_w – wall shear stress

φ – stream function

Subscripts

w – wall

∞ – free stream

References

[1] Jilani G., Jayaraj S. and Ahmad M.A. (2002): *Conjugate forced convection–conduction heat transfer analysis of a heat generating vertical cylinder*.– International Journal of Heat and Mass Transfer, vol. 45, pp.331-341, https://doi.org/10.1016/S0017-9310(01)00140-5.

[2] Rani H. and Reddy G.J. (2011): *Conjugate transient free convective heat transfer from a vertical slender hollow cylinder with heat generation effect*.– Appl. Math, vol.1, pp.90-98, https://doi.org/10.5923/j.am.20110102.15.

[3] Kaya Ahmet (2011): *The effect of conjugate heat transfer on MHD mixed convection about a vertical slender hollow cylinder*.– Communications in Nonlinear Science and Numerical Simulation, vol.16, pp.1905-1916, https://doi.org/10.1016/j.cnsns.2010.08.021.

[4] Lukaszewicz G. (1999): *Micropolar Fluids: Theory and Applications*.– Springer Science & Business Media, https://link.springer.com/book/10.1007/978-1-4612-0641-5.

[5] Eringen A.C. (1966): *Theory of micropolar fluids*.– Journal of Mathematics and Mechanics, pp.1-18.

[6] Eringen A.C. (1972): *Theory of thermomicrofluids*.– Journal of Mathematical Analysis and Applications, vol.38, pp.480-496, https://doi.org/10.1016/0022-247X(72)90106-0.

[7] Ariman T., Turk M. and Sylvester N. (1973): *Microcontinuum fluid mechanics-a review*.– International Journal of Engineering Science, vol.11, pp.905-930, https://doi.org/10.1016/0020-7225(73)90038-4.

[8] Ariman T., Turk M. and Sylvester N. (1974): *Applications of microcontinuum fluid mechanics*.– International Journal of Engineering Science, vol.12, pp.273-293, https://doi.org/10.1016/0020-7225(74)90059-7.

[9] Gorla R.S.R. and Takhar H. (1987): *Free convection boundary layer flow of a micropolar fluid past slender bodies*.– International Journal of Engineering Science, vol.25, pp.949-962, https://doi.org/10.1016/0020-7225(87)90090-5.

[10] Gorla R.S.R. (1989): *Combined forced and free convection in the boundary layer flow of a micropolar fluid on a continuous moving vertical cylinder*.– International Journal of Engineering Science, vol.27, pp.77-86, https://doi.org/10.1016/0020-7225(89)90169-9.

[11] Chang C.-L. (2006): *Buoyancy and wall conduction effects on forced convection of micropolar fluid flow along a vertical slender hollow circular cylinder*.– International Journal of Heat and Mass Transfer, vol.49, pp.4932-4942, https://doi.org/10.1016/j.ijheatmasstransfer.2006.05.037.

[12] Siddiqa S., Begum N., Md Hossain A., Abrar M.N., Gorla R.S.R. and Al-Mdallal Q. (2021): *Effect of thermal radiation on conjugate natural convection flow of a micropolar fluid along a vertical surface*.– Computers & Mathematics with Applications, vol.83, pp.74-83, https://doi.org/10.1016/j.camwa.2020.01.011.

[13] Bhargava R. and Rana P. (2011): *Finite element solution to mixed convection in MHD flow of micropolar fluid along a moving vertical cylinder with variable conductivity*.– Int. J. Appl. Math. Mech, vol.7, pp.29-51.

[14] Sivarami Reddy C., Ramachandra Prasad V. and Jayalakshmi K. (2021): *Numerical simulation of natural convection heat transfer from a heated square cylinder in a square cavity filled with micropolar fluid*.– Heat Transfer, vol.50, pp.5267-5285, https://doi.org/10.1002/htj.22123.

[15] Saidoune F., Bouaziz M. and Aziz A. (2021): *Conjugate heat and mass transfer on steady mhd mixed convection flow along a vertical slender hollow cylinder with heat generation and chemical reaction effects*.– Defect and Diffusion Forum, Trans. Tech. Publ., vol.406, pp.53-65, https://doi.org/10.4028/www.scientific.net/DDF.406.53.

[16] Alwawi F., Sulaiman I.M., Al-Swalmeh M.Z. and Yaseen N. (2022): *Energy transport boosters of magneto micropolar fluid flowing past a cylinder: A case of laminar combined convection*.– Proceedings of the Institution of Mechanical Engineers, Part C: Journal of Mechanical Engineering Science, vol.236, pp.10902-10913, https://doi.org/10.1177/09544062221111055.

[17] Hassan H., Regnier N., Pujos C. and Defaye G. (2008): *The effect of viscous dissipation on the polymer temperature during injection molding*.– Proceedings of the 5th European Thermal-Sciences Conference, vol.48, No.6, pp.1199-1206.

[18] Kaya A. and Aydin O. (2014): *Combined Effect of Viscous Dissipation on the Coupling of Conduction and Mixed Convection Along a Vertical Slender Hollow Cylinder*.– Progress in Exergy, Energy, and the Environment, pp.595-607, https://doi.org/10.1007/978-3-319-04681-5_56.

[19] Anantha Kumar K., Sugunamma V. and Sandeep N. (2020): *Influence of viscous dissipation on MHD flow of micropolar fluid over a slendering stretching surface with modified heat flux model*.– Journal of Thermal Analysis and Calorimetry, vol.139, pp.3661-3674, https://doi.org/10.1007/s10973-019-08694-8.

[20] Lund L.A., Zurni O., Ilyas K., Jawad R., El-Sayed M.S. and Asiful H.S. (2020): *Magnetohydrodynamic (MHD) flow of micropolar fluid with effects of viscous dissipation and joule heating over an exponential shrinking sheet: triple solutions and stability analysis*.– Symmetry, vol.12, pp.142, https://doi.org/10.3390/sym12010142.

[21] Kataria H.R., Mistry M. and Mittal A. (2022): *Influence of nonlinear radiation on MHD micropolar fluid flow with viscous dissipation*.– Heat Transfer, vol.51, pp.1449-1467, https://doi.org/10.1002/htj.22359.

[22] Waini I., Ishak A. and Pop I. (2022): *Radiative and magnetohydrodynamic micropolar hybrid nanofluid flow over a shrinking sheet with Joule heating and viscous dissipation effects*.– Neural Computing and Applications, vol.34, pp.3783-3794, https://doi.org/10.1007/s00521-021-06640-0.

[23] Alliche S.A. and Bouaziz M.N. (2018): *Magnetic field and thermal radiation effects on mixed convection heat and mass transfer of micropolar fluid along a vertical slender hollow circular cylinder*.– JP Journal of Heat and Mass Transfer, vol.15, pp.157-180, http://dx.doi.org/10.17654/HM015020157.

[24] Shampine L.F., Kierzenka J. and Reichelt M.W. (2000): *Solving boundary value problems for ordinary differential equations in MATLAB with bvp4c*.– Tutorial notes 2000, pp.1-27.

[25] Mucoglu A. and Chen T. (1976): *Buoyancy effects on forced convection along a vertical cylinder with uniform surface heat flux*.– J. Heat Transfer, vol.98, pp.523-525, https://doi.org/10.1115/1.3450591.

Received: November 11, 2023
Revised: January 17, 2024